ROYAL SOCIETY
OF CHEMISTRY

PAPER

Check for updates

Operando quantification of diffusion-induced stresses in O3-type NaNi$_{1/3}$Fe$_{1/3}$Mn$_{1/3}$O$_2$ sodium-ion battery electrode during electrochemical cycling†

Amit Chanda,[a] Daniel P. Abraham, [ID] [b] Stephen E. Trask [ID] [b] and
Siva P. V. Nadimpalli [ID] *[a]

The extraction and insertion of Na$^+$ ions into transition metal layered oxides based on Ni, Fe, and Mn (NFM) can introduce stresses in electrode coatings containing these materials. The magnitude and nature of such stresses generated in an NaNi$_{1/3}$Fe$_{1/3}$Mn$_{1/3}$O$_2$ (NFM111) electrode are investigated in this study using the substrate curvature method. A complex profile comprising both tensile and compressive stresses are observed during the electrochemical desodiation/sodiation cycles in a Na metal counter electrode cell. The peak compressive and tensile stresses experienced by the electrode during cycling in the 2.0–4.1 V range are − 4 MPa and 2.7 MPa, respectively. Similar stress profiles are obtained from measurements in two different in-plane directions, indicating that the response is an average of randomly oriented particles in the electrode coating. The stress evolution shows excellent correlations with phase changes in the oxide that result from removal and insertion of the alkali ions. The experimental data are being used to develop mechanically durable NFM electrodes for high-performance sodium-ion batteries intended for transportation and electricity-grid applications.

Broader context

Sodium-ion batteries (SIBs) containing layered oxide cathodes have emerged as a promising alternative to lithium-ion batteries (LIBs). Although layered oxide cathodes include advantages such as high theoretical capacity and relative ease of synthesis, phase transitions, and stress-induced mechanical degradation possess challenge towards improved electrochemical performance. The mechanical durability becomes especially crucial during cycling at the high voltages to make SIB cells cost-competitive with LIB cells. Understanding and measuring the stresses generated during the (de)intercalation of sodium ions from (into) the oxide structure is critical for improving the mechanical durability and electrochemical performance of SIB cells with metal oxide cathodes. In response to these challenges, this study focuses on operando stress measurements on commercially relevant high-capacity sodium-ion battery electrodes (NFM) during electrochemical cycling. The experimental data shows excellent correlations between stress evolution and phase changes in the oxide and can be used to develop mechanically durable NFM electrodes for high-performance sodium-ion batteries intended for transportation and electricity-grid applications.

1. Introduction

Sodium-ion batteries (SIBs) containing O3-type layered oxides such as NaNi$_x$Fe$_y$Mn$_z$O$_2$ (NFM) have emerged as a promising alternative to lithium-ion batteries (LIBs) with lithium iron phosphate (LFP)-based cathodes.[1–3] Advantages of the NFM

[a]Department of Mechanical Engineering, Michigan State University, 428 S. Shaw Lane, East Lansing, MI, 48824, USA. E-mail: sivan@msu.edu
[b]Chemical Sciences and Engineering Division, Argonne National Laboratory, Lemont, Illinois, 60439, USA

oxides include their high theoretical capacity and relative ease of synthesis; disadvantages include phase transitions and stress-induced mechanical degradation, especially during cycling at the high voltages needed to make SIB cells cost-competitive with LIB cells.[4] Understanding and measuring the stresses generated during the (de)intercalation of sodium ions from (into) the oxide structure is critical for improving the electrochemical performance and cycle life of SIB cells with NFM cathodes.

Whereas several methods have been employed to monitor structural and oxidation-state changes in O3-type layered oxides,[4–10] few techniques are available for the measurement of stresses during electrochemical cycling. One such technique

is the substrate-curvature method, which has been employed to examine diffusion-induced stresses in electrodes used as anodes and cathodes in LIB cells.[11–15] For instance, Nadimpalli *et al.*[12] measured real-time stress evolution in a porous electrode containing $Li_{1.2}Ni_{0.15}Mn_{0.55}Co_{0.1}O_2$ and showed that the stress evolution profile could be correlated with the phase evolution profile obtained from *in situ* X-ray diffraction studies on the material. Fewer wafer curvature studies exist on composite electrodes developed for SIB cells, although the technique has been extensively used to examine (de)sodiation stresses in thin films electrodes.[16,17]

In this study, we conduct operando stress measurements on commercially relevant high-capacity $NaNi_{1/3}Fe_{1/3}Mn_{1/3}O_2$ (NFM111) electrodes during electrochemical cycling. The optical-based substrate-curvature method is employed to obtain real-time stresses developed in the electrode during the initial electrolyte wetting period and the following (de)sodiation cycles. The unique features of the stress patterns are correlated with the complex structural transformation and volume changes in the material that are reported in the research literature. These measurements are intended to complement studies being conducted at Argonne National Laboratory (ANL) to examine the physicochemical mechanisms that lead to electrochemical performance degradation during long-term aging of SIB cells. Data from these characterization techniques are intended to enable design strategies that enhance the structural stability of NFM-based cathodes and improve cycle life of high-performance cells being developed for transportation and large-scale energy storage applications.

Additional table and figures to complement and enhance data shown in the main text are available in the ESI;† these have the designator ESI† in this manuscript.

2. Experimental

2.1. Cell assembly – materials and electrochemical methods

The O3-type $NaNi_{1/3}Fe_{1/3}Mn_{1/3}O_2$ (NFM111) electrodes examined in this study are from the cell analysis, modeling and prototyping (CAMP) facility at ANL. The oxide secondary particles (Fig. 1a) are between 5–20 μm in size, with a D_{50} of ~10 μm. The primary particles (that are sintered together to form the secondary) have a faceted morphology and range in size from 0.2–1 μm. The electrode (Table S1†) comprises a coating of commercial NFM111 (95 wt%), C45 carbon (2.95 wt%), single walled carbon nanotubes (SWCNT, 0.05 wt%) and PVdF binder (2 wt%) on a 20 μm thick Al current collector. The electrode coating thickness is 136 μm and the porosity is estimated as 34.4% (see Section S1 of the ESI† for details about porosity estimation). In coin cell tests, the electrodes show capacity-voltage profiles (Fig. 1b) that are typical of NFM111 and display areal capacities of ~5 mA h cm^{-2} (~135 mA h g^{-1}, 2.0–4.1 V range, C/25 rate). The capacities are lower at higher cycling rates (Fig. S2†): the capacity decrease denotes a higher cell impedance that includes contributions from the Na-metal
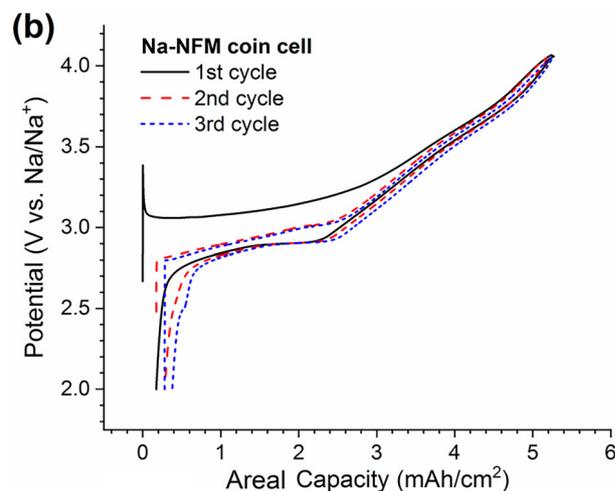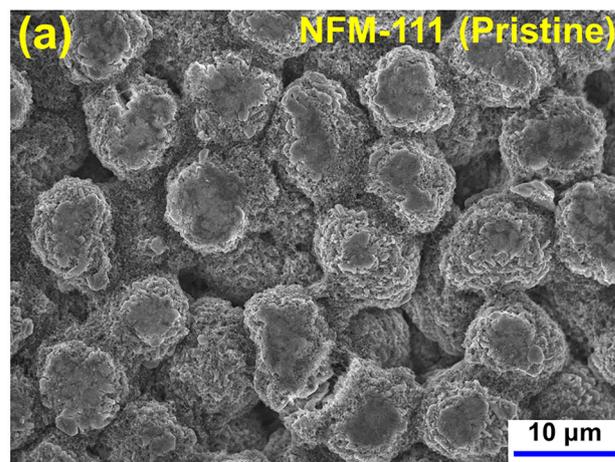
Fig. 1 (a) Scanning electron microscopy (SEM) image of the pristine NFM111 electrode. (b) Potential *vs.* areal capacity data from a coin cell containing the NFM111 electrode and Na-metal counter electrode: data for the first 3 cycles at ~C/25 rate are shown.

counter electrode that degrades over time because of the plating/stripping cycles (discussed later).

For the stress measurements, the NFM111 electrode (20.26 cm^2) is cycled against sodium metal in a beaker cell assembled and tested inside an inert-atmosphere glovebox. Details of the cell assembly are shown in Fig. S3.† In brief, the Na foil with embedded Cu-wire (which serves as the cell anode) is placed in a Teflon beaker. The Al current collector of the NFM111 electrode is bonded to the rough side of a polished Si (111) wafer and placed on the Na foil, with a glass fiber separator in-between to prevent physical contact. The electrolyte comprises 1 M $NaClO_4$ salt in propylene carbonate (PC) solvent and 5 wt% fluoroethylene carbonate (FEC) as the additive. The beaker is sealed with a stainless-steel lid that has a glass window to allow ingress and egress of laser beams. After assembly, the electrochemical cell rests at open circuit voltage (OCV) for ~8 h to allow complete wetting of the electrodes: then, cycling is conducted between 2 and 4.1 V *vs.* Na with a current of 0.2 mA cm^{-2} (~C/25 rate).

2.2. Stress evaluation through substrate curvature measurements

The in-plane expansion/contraction of electrode coating during wetting by the electrolyte and electrochemical cycling is constrained by the elastic substrate which induces equi-biaxial stress fields in the electrode (as shown in schematic Fig. S1 of ESI†). Curvature changes of the Si substrate during wetting and cycling are recorded with a multi-beam optical sensing (MOS, k space associates, USA) system, shown in the schematic of Fig. 2. The MOS system utilizes an array of laser beams that get reflected from the polished surface of the Si substrate and are captured in a CCD camera. The change in substrate curvature is obtained from relative changes in the laser spot spacing and can be expressed as,

$$\kappa = \frac{1}{A_m} \frac{d - d^0}{d^0}, \tag{1}$$

where d and d^0 are the instantaneous and initial distance between adjacent laser spots, respectively, and A_m is the mirror constant which is experimentally measured as 1.6 m. The measured curvature, κ, is related to the average electrode stress using the modified Stoney's[11,18] equation as,

$$\sigma = \frac{M_s t_s{}^2 \kappa}{6 t_f f(t_i, M_i)} \tag{2}$$

where M_s and t_s are bi-axial modulus and thickness of the Si substrate, t_f is the electrode thickness and $f(t_i, M_i)$ is the function of thickness and bi-axial modulus of all layers (see Fig. 2 inset). Note that the original Stoney equation was developed for stress measurement in films that are much thinner than the substrate. In this study, the electrode coating cannot be considered as a thin film, and two additional layers (Al current collector and epoxy) are also present. Hence, eqn (2), which is a modified formula that considers elastic properties of each layer is used for the stress calculation.[11] Details of material properties used for these calculations are shown in Table 1.

3. Results and discussion

3.1. Initial stress evolution during cell OCV (electrode wetting effects)

Stress evolution in the NFM111 electrode after electrolyte addition, but prior to any electrochemical cycling, is shown in Fig. S4a.† The stress starts at zero then increases gradually with time, reaching ~0.3 MPa of tensile stress around 4 h: note that the tensile and compressive stresses are represented with positive and negative values, respectively. It is apparent that the absorption of electrolyte generates tensile stresses, which indicates shrinking of the electrode coating. A similar tensile stress was also observed during electrolyte-wetting of hard carbon electrodes being developed as anodes for SIB cells.[13] The observed stress can be attributed to the complex interaction between electrode pores and electrolyte due to surface tension. Here, surface tension refers to the force acting at the electrolyte-particle interface within the electrode pore trying to minimize the surface area: the stress is from elastic deformation of pore walls because of forces that include the surface
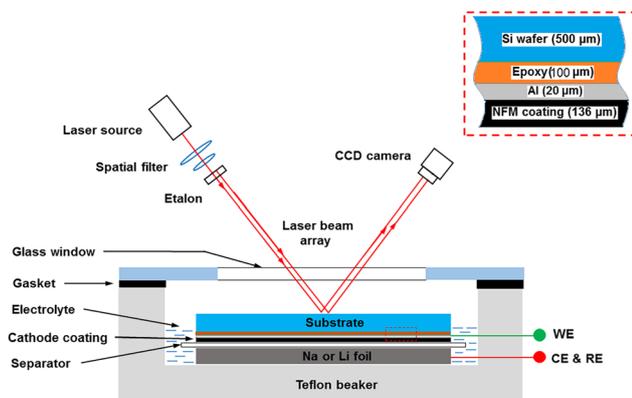

Fig. 2 Schematic of beaker cell used for substrate curvature measurements. The inset shows the electrode bonding to the substrate along with thickness values of individual layers.

**Table 1** Material parameters used for stress calculation

Parameter	Definition	Value	Comments
Si (111) wafer			
E_1	Young's modulus	169 GPa	Ref. 19
ν_1	Poisson's ratio	0.26	Ref. 19
h_1	Thickness	500 μm	Measured
Epoxy adhesive			
E_2	Young's modulus	4.3 GPa	Ref. 11
ν_2	Poisson's ratio	0.36	Ref. 11
h_2	Thickness	100 μm	Measured
Aluminum collector			
E_3	Young's modulus	67.3 GPa	Ref. 13
ν_3	Poisson's ratio	0.33	Ref. 13
h_3	Thickness	20 μm	Measured
NFM111 composite			
E_4	Young's modulus	13.72 GPa	Calculated, rule of mixture
ν_4	Poisson's ratio	0.2	Calculated, rule of mixture
h_4	Thickness	136 μm	Measured

tension.[20,21] In smaller pores, surface tension plays a significant role in generating stress due to increased curvature of the liquid interface. Hence, electrode properties such as pore size and tortuosity, and material properties such as wettability of the oxide and binder influence the surface tension and, therefore, magnitude of the observed stress.

3.2. Stress evolution in NFM111 during galvanostatic cycling

The potential and stress response of the NFM111 electrode during the first two galvanostatic cycles are shown in Fig. 3a. During the 1st cycle, the charge (desodiation) capacity is ~5.5 mA h cm^{-2} while the discharge (sodiation) capacity is ~5 mA h cm^{-2} resulting in a coulombic efficiency (CE) of ~90%. The potential profile for this cycle shows an initial voltage spike to 3.4 V *vs.* Na, which is attributed to the decomposition of surface impurities (such as Na_2CO_3) on the oxide; the potential decreases after decomposition of these impurities. The subsequent charge/discharge profile is similar to the coin cell data (Fig. 1b) and consistent with data reported in the research literature.[5,6]
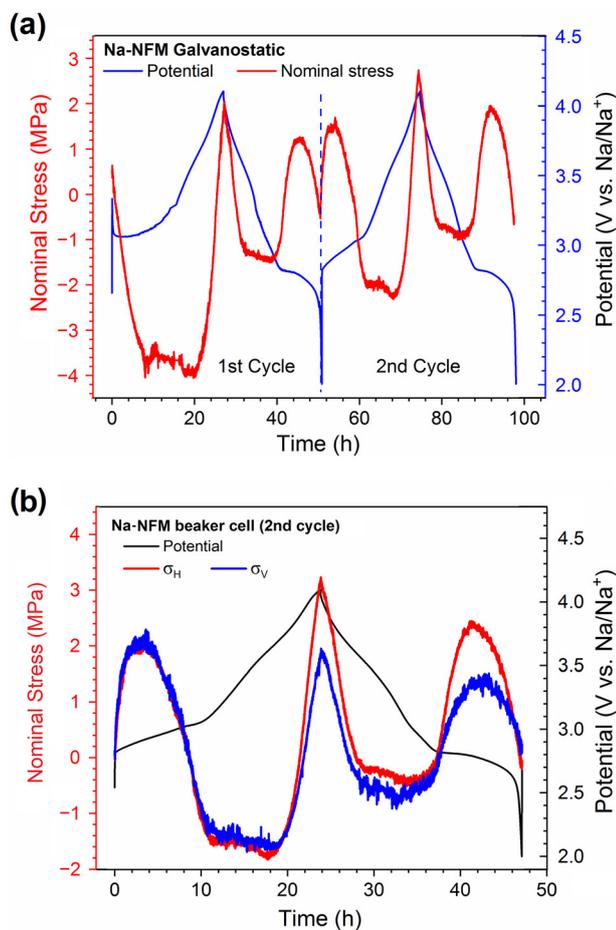
The stress profile during the 1st charge is different from that of subsequent cycles (Fig. 3a). The stress decreases almost linearly from a tensile value of ~0.55 MPa (at 2.7 V) and becomes compressive, reaching −4 MPa at ~8 h (3.1 V); the values fluctuate between −3.5 and −4 MPa for the next 12 h. After 20 h the stress changes direction and increases rapidly, reaching a tensile value of 2 MPa at ~27 h (4.1 V, top of charge). During discharge, as the cell potential decreases, the stress decreases rapidly and becomes compressive with a value about −1.2 MPa around 32 h, then decreases gradually to −1.5 MPa around 38 h (2.98 V). Then the stress increases, reaching a peak tensile value of 1.2 MPa at ~45 h (2.78 V), followed by a decrease to −0.54 MPa at the bottom of charge (2.0 V). The complex stress profile is repeated in subsequent cycles, as seen in Fig. 3a and Fig. S4b.† The peak compressive stress measured in this NFM111 electrode (−4 MPa) is slightly lower than the −6 MPa value reported for the Li-rich NMC electrode in[12] but the peak tensile stress here (2 MPa) is higher than the 1 MPa reported therein. These peak values are affected by multiple factors that include properties of the electrode materials (oxide, carbons, binder) and characteristics of the electrode (porosity, tortuosity, *etc.*).

The in-plane stresses (σ_H and σ_V) in two orthogonal directions of the electrode coating (Fig. 3b) are very similar: that is, the electrode coating shows an isotropic stress response. Although the volume change behavior of individual oxide particles is anisotropic, the average volume change response of the composite electrode is isotropic, indicating that the particles are randomly oriented. Some deviation is observed between the σ_H and σ_V values, especially during the 2nd discharge. This deviation is attributed to changes in the Na-metal foil because of the plating/stripping processes (Fig. S5†), which creates uneven surfaces and alters the measured curvatures. To test this attribution, the beaker cell was disassembled after 3 cycles and a fresh Na-foil used for subsequent cycles. The resulting data (Fig. S6†) showed very similar σ_H and σ_V values, thereby confirming our Na foil degradation hypothesis.

3.3. Correlating stress evolution to structural changes in NFM111 during cycling

The NFM crystal structure contain sheets of edge-sharing (TM) O_6 octahedra, where TM = transition metal (here Ni, Fe, Mn) and O is oxygen.[22,23] Polymorphs appear when these sheets are stacked in different orientations along the *c*-axis. The main polymorphs are of the O-type and P-type in which the Na$^+$ ions are present in octahedral (O) and prismatic (P) sites, respectively. The number of sheets within the unit cells (2 or 3), also determines the structural types, which include P3, P2 and O3. The pristine NFM111 exhibits the O3 structure.[4,5,24] The Na interlayer spacing changes with increasing Na$^+$ extraction from the oxide, yielding in sequence the O3–H2, P3, OP2 structures: charge compensation until ~0.7 Na$^+$ extraction is mainly provided by the oxidation of Ni^{2+} to Ni^{4+}.[4] At higher levels of desodiation, the material exhibits an intergrowth of OP2 and O3 structures: as per the earlier reports,[4,8,24] charge compensation results from the Fe^{3+} to Fe^{4+} oxidation. Reversibility of the

Fig. 3 (a) Stress and potential evolution of NFM111 electrode as a function of time during first two galvanostatic cycles; (b) evolution of the in-plane stresses in two orthogonal directions during the 2nd galvanostatic cycle; σ_H and σ_V signifies stresses in the *x*- and *y*-directions, respectively.

intercalation process suffers when the extent of desodiation exceeds ~0.65 because of Fe migration to the alkali metal layers.[25]

The complex stress evolution in NFM111, as a function of electrode potential and extent of desodiation (x) during the 2nd cycle, is shown in Fig. 4a; the differential capacity (dQ/dV) trends are in Fig. 4b. The same data, plotted with areal capacity on the X-axis, are displayed in Fig. S7a and b.† In general, the stress evolution plot can be divided into 4 stages (Fig. 4a). In stage 1 during charge (Na$^+$ extraction), the stress increases with voltage reaching a peak tensile value of ~1.5 MPa at a potential of ~2.9 V $vs.$ Na and $x \approx 0.158$; the tensile value indicates shrinkage in the electrode coating. Thereafter, in stage 2, the stress decreases almost linearly, reaching a compressive value of around −2 MPa at a potential of ~3.1 V $vs.$ Na and $x \approx 0.32$; the compressive value indicates expansion in the electrode coating. On further Na$^+$ extraction (stage 3) the stress is mostly constant, increasing slightly to around −2.3 MPa at a potential of ~3.6 V $vs.$ Na and $x \approx 0.48$. Beyond 3.6 V (stage 4), the stress increases rapidly, changing from compressive to tensile and reaching 2.7 MPa at a potential of 4.1 V $vs.$ Na and $x \approx 0.61$; that is the expanded coating (at end of stage 3) shrinks rapidly during stage 4.

Similar stages are seen during discharge, during which Na$^+$ is inserted into the oxide structure and electrode potential decreases: the processes mostly occur in reverse, with an obvious offset in the magnitude of the observed stress. The stress decreases to −0.75 MPa at the end of stage 4 (3.5 V $vs.$ Na and $x \approx 0.48$), then remains almost constant till the end of stage 3 (2.85 V $vs.$ Na and $x \approx 0.32$), reaches a peak tensile value of 1.9 MPa (2.8 V $vs.$ Na and $x \approx 0.22$), then decreases to a compressive value of −0.7 MPa (2.0 V $vs.$ Na and $x \approx 0.09$) in stage 1.

It is evident that during the electrochemical cycling the electrode experiences repeated contractions and expansions, which can affect cohesion of the coating components and adhesion between the coating and the Al foil. The former can degrade connectivity between the oxide particles and the carbon (electron conduction) network: the latter can, in extreme cases, cause coating debonding from the current collector. That is, the cycling stresses can cause mechanical degradation, which will affect electrochemical performance through an increase in impedance (through resistivity increases) and a decrease in capacity (through active material losses). Clearly, high-performance binders are needed to absorb stresses generated by repeated volume changes and mitigate mechanical degradation of the coating.

The NFM111 stress evolution can be compared to the reported[4,5,26] phase evolution and crystal structure changes in the oxide during (de)sodiation cycles: note that the phase evolution features are also seen in the differential capacity plots (Fig. 4b). See also the remarkable correspondence between the stress generated and unit cell volume changes of the oxide in Fig. S8.† During stage 1 of desodiation, the O3–H1 polymorph transforms to a related O3–H2 structure. Stage 2 corresponds to a transformation of O3–H2 to the P3 structure. O3 and P3 likely coexist in stage 2 as the transformation is slow, apparently because of the significant lattice mismatch between the phases. In Stage 3, which could be considered an extension of stage 2, the P3 structure completely replaces O3. Upon further desodiation (stage 4), the OP2 begins to appear, initially co-existing with and eventually replacing P3. These structural changes occur in reverse during the sodiation. Note that the extent of desodiation (Fig. 4a and b) is less than 0.61, thereby ensuring reversibility of the crystal structure changes.

The stress hysteresis observed between the charge and discharge cycles could be from subtle differences in phase contents for a given level of (de)sodiation and/or from mechanical dissipation processes in the polymer (PVdF) binder. Further studies are needed to de-convolute contribution of the binder to the stress evolution. Microstructural examination of the NFM electrodes after about 5 cycles showed no obvious damage to the oxide particles or the PVdF binder: the latter apparently possesses the characteristics needed to mitigate coating degradation, at least for a limited number of cycles.
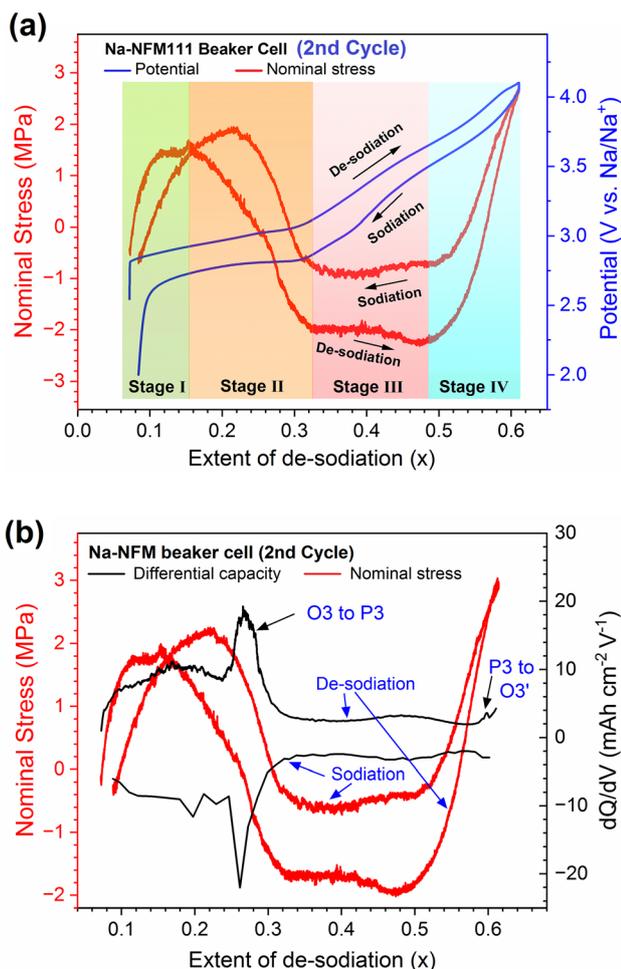

Fig. 4 (a) Stress and potential evolution of NFM111 electrode during Na$^+$ extraction/insertion into the oxide showing various stress stages during the 2nd cycle. (b) Corresponding differential capacity plots overlaid on the stress response.

Additional examination of highly-aged electrodes is planned to examine the role of mechanical degradation in cell performance loss. The contribution of mechanical processes could become even more significant for NFM electrodes in SIBs that are cycled to the higher voltages needed to achieve specific energies and energy densities comparable to those of LFP-bearing LIB cells.

4. Conclusions

Real-time stress evolution in a composite $NaNi_{1/3}Fe_{1/3}Mn_{1/3}O_2$ (NFM111) electrode is obtained with the substrate-curvature technique in a custom-made beaker cell during the first few galvanostatic (de)sodiation cycles in the 2.0–4.1 V *vs.* Na range. The potential and capacity data from the beaker cell are comparable to that of an analogous coin cell. The conclusions from the experiments are as follows.

• The NFM111 electrode exhibits a complex nonlinear stress profile during cycling: both compressive and tensile stresses are observed during each desodiation and sodiation portions of the cycle. The stress profile during the 1st first desodiation half-cycle is different from that of subsequent cycles. The peak compressive stress exhibited by the electrode is ~4 MPa, whereas the peak tensile stress is ~2.7 MPa.

• The electrode shows an isotropic stress response, as seen from the similar profiles in two different in-plane directions, indicating that the response is an average of randomly oriented particles in the coating.

• The stress signatures correlate well with the various structural transitions in the NFM111 oxide seen in XRD data reported in the research literature.

This study provides important information about stress evolution in a commercially relevant sodium-ion battery electrode. The data can be used in models being developed to predict aging behavior and lifespan of SIB cells. The substrate-curvature technique can also be used as a diagnostic tool to investigate the complex structure–property correlations in NFM electrodes.

Data availability

Data supporting the findings of this study are included in the main manuscript and the ESI.†

Conflicts of interest

There are no conflicts to declare.

Acknowledgements

References

1 N. Yabuuchi, K. Kubota, M. Dahbi and S. Komaba, Research Development on K-Ion Batteries, *Chem. Rev.*, 2020, **120**(14), 6358–6466, DOI: **10.1021/acs.chemrev.9b00463**.

2 T. Song, L. Chen, D. Gastol, B. Dong, J. F. Marco, F. Berry, P. Slater, D. Reed and E. Kendrick, High-Voltage Stabilization of O3-Type Layered Oxide for Sodium-Ion Batteries by Simultaneous Tin Dual Modification, *Chem. Mater.*, 2022, **34**(9), 4153–4165, DOI: **10.1021/acs.chemmater.2c00522**.

3 S. Zhao, Q. Shi, W. Feng, Y. Liu, X. Yang, X. Zou, X. Lu and Y. Zhao, Research Progresses in O3-Type Ni/Fe/Mn Based Layered Cathode Materials for Sodium Ion Batteries, *Carbon Neutrality*, 2023, **2**, 13, DOI: **10.1007/s43979-023-00053-9**.

4 K. Fang, J. Yin, G. Zeng, Z. Wu, Y. Tang, D. Yu, H. Luo, Q. Liu, Q. Zhang, T. Qiu, H. Huang, Z. Ning, C. Ouyang, L. Gu, Y. Qiao and S. G. Sun, Elucidating the Structural Evolution of O3-Type NaNi1/3Fe1/3Mn1/3O2: A Prototype Cathode for Na-Ion Battery, *J. Am. Chem. Soc.*, 2024, **146**, 31860–31872, DOI: **10.1021/jacs.4c11049**.

5 Y. Xie, H. Gao, R. Harder, L. Li, J. Gim, H. Che, H. Wang, Y. Ren, X. Zhang, L. Li, Z. Chen, K. Amine and Z. F. Ma, Revealing the Structural Evolution and Phase Transformation of O3-Type NaNi1/3Fe1/3Mn1/3O2 Cathode Material on Sintering and Cycling Processes, *ACS Appl. Energy Mater.*, 2020, **3**(7), 6107–6114, DOI: **10.1021/acsaem.0c00475**.

6 D. Kim, E. Lee, M. Slater, W. Lu, S. Rood and C. S. Johnson, Layered Na[Ni 1/3Fe 1/3Mn 1/3]O 2 Cathodes for Na-Ion Battery Application, *Electrochem. Commun.*, 2012, **18**(1), 66–69, DOI: **10.1016/j.elecom.2012.02.020**.

7 A. Sengupta, A. Kumar, G. Barik, A. Ahuja, J. Ghosh, H. Lohani, P. Kumari, T. K. Bhandakkar and S. Mitra, Lower Diffusion-Induced Stress in Nano-Crystallites of P2-Na2/3Ni1/3Mn1/2Ti1/6O2 Novel Cathode for High Energy Na-Ion Batteries, *Small*, 2023, **19**(12), 1–15, DOI: **10.1002/smll.202206248**.

8 V. A. Shevchenko, I. S. Glazkova, D. A. Novichkov, I. Skvortsova, A. V. Sobolev, A. M. Abakumov, I. A. Presniakov, O. A. Drozhzhin and E. V. Antipov, Competition between the Ni and Fe Redox in the O3-NaNi1/3Fe1/3Mn1/3O2 Cathode Material for Na-Ion

Batteries, *Chem. Mater.*, 2023, **35**(10), 4015–4025, DOI: **10.1021/acs.chemmater.3c00338**.

9 D. Schäfer, K. Hankins, M. Allion, U. Krewer, F. Karcher, L. Derr, R. Schuster, J. Maibach, S. Mück, D. Kramer, R. Mönig, F. Jeschull, S. Daboss, T. Philipp, G. Neusser, J. Romer, K. Palanisamy, C. Kranz, F. Buchner, R. J. Behm, A. Ahmadian, C. Kübel, I. Mohammad, A. Samoson, R. Witter, B. Smarsly and M. Rohnke, Multiscale Investigation of Sodium-Ion Battery Anodes: Analytical Techniques and Applications, *Adv. Energy Mater.*, 2024, **14**(15), 2302830, DOI: **10.1002/aenm.202302830**.

10 D. Hou, D. Xia, E. Gabriel, J. A. Russell, K. Graff, Y. Ren, C. J. Sun, F. Lin, Y. Liu and H. Xiong, Spatial and Temporal Analysis of Sodium-Ion Batteries, *ACS Energy Lett.*, 2021, **6**(11), 4023–4054, DOI: **10.1021/acsenergylett.1c01868**.

11 V. A. Sethuraman, N. Van Winkle, D. P. Abraham, A. F. Bower and P. R. Guduru, Real-Time Stress Measurements in Lithium-Ion Battery Negative-Electrodes, *J. Power Sources*, 2012, **206**, 334–342, DOI: **10.1016/j.jpowsour.2012.01.036**.

12 S. P. V. Nadimpalli, V. A. Sethuraman, D. P. Abraham, A. F. Bower and P. R. Guduru, Stress Evolution in Lithium-Ion Composite Electrodes during Electrochemical Cycling and Resulting Internal Pressures on the Cell Casing, *J. Electrochem. Soc.*, 2015, **162**(14), A2656–A2663, DOI: **10.1149/2.0341514jes**.

13 A. Chanda, A. Pakhare, A. Alfadhli, V. A. Sethuraman and S. P. V. Nadimpalli, Real-Time Measurement of Sodiation Induced Stress in Hard Carbon Composite Electrodes, *J. Power Sources*, 2024, **609**, 234678, DOI: **10.1016/j.jpowsour.2024.234678**.

14 H. Jiang, J. Chen, X. Li, Z. Jin, T. Chen, J. Liu and D. Li, A Comprehensive Review of In Situ Measurement Techniques for Evaluating the Electro-Chemo-Mechanical Behaviors of Battery Electrodes, *Molecules*, 2024, **29**(8), 1873, DOI: **10.3390/molecules29081873**.

15 A. Mukhopadhyay, A. Tokranov, X. Xiao and B. W. Sheldon, Stress Development Due to Surface Processes in Graphite Electrodes for Li-Ion Batteries: A First Report, *Electrochim. Acta*, 2012, **66**, 28–37, DOI: **10.1016/j.electacta.2012.01.058**.

16 S. Rakshit, A. S. Pakhare, O. Ruiz, M. R. Khoshi, E. Detsi, H. He, V. A. Sethuraman and S. P. V. Nadimpalli, Measurement of Volume Changes and Associated Stresses in Ge Electrodes Due to Na/Na + Redox Reactions, *J. Electrochem. Soc.*, 2021, **168**(1), 010504, DOI: **10.1149/1945-7111/abd5fc**.

17 P. Gandharapu, A. Das, R. Tripathi, V. Srihari, H. K. Poswal and A. Mukhopadhyay, Facile and Scalable Development of High-Performance Carbon-Free Tin-Based Anodes for Sodium-Ion Batteries, *ACS Appl. Mater. Interfaces*, 2023, **15**(31), 37504–37516, DOI: **10.1021/acsami.3c07305**.

18 G. G. Stoney, The Tension of Metallic Films Deposited by Electrolysis, *Nature*, 1909, 366.

19 W. A. Brantley, Calculated Elastic Constants for Stress Problems Associated with Semiconductor Devices, *J. Appl. Phys.*, 1973, **44**(1), 534–535, DOI: **10.1063/1.1661935**.

20 D. Kramer and J. Weissmuller, A Note on Surface Stress and Surface Tension and Their Interrelation via Shuttleworth ' s Equation and the Lippmann Equation, *Surf. Sci.*, 2007, **601**, 3042–3051, DOI: **10.1016/j.susc.2007.05.005**.

21 G. Y. Gor, P. Huber and J. Weissmüller, Elastocapillarity in Nanopores : Sorption Strain from the Actions of Surface Tension and Surface Stress, *Phys. Rev. Mater.*, 2018, **2**, 086002, DOI: **10.1103/PhysRevMaterials.2.086002**.

22 L. Su, B. Sun, M. Wu, G. Liu, B. Xu and C. Ouyang, Structural and Na-Ion Diffusion Behavior of O3/P3/P2-Type NaNi$_{1/3}$Mn$_{1/3}$Fe$_{1/3}$O$_2$ Cathode for Na-Ion Batteries from First- Principles Study, *J. Chem. Phys.*, 2024, **160**, 064703, DOI: **10.1063/5.0187281**.

23 C. Delmas, J.-J. Braconnier, C. Fouassier and P. Hagenmuller, Electrochemical Intercalation of Sodium in NaxCoO2 Bronzes, *Solid State Ionics*, 1981, **3–4**, 165–169.

24 M. Jeong, H. Lee, J. Yoon and W. Yoon, O3-Type NaNi$_{1/3}$Fe$_{1/3}$Mn$_{1/3}$O$_2$ Layered Cathode for Na-Ion Batteries : Structural Evolution and Redox Mechanism upon Na (de) Intercalation, *J. Power Sources*, 2019, **439**, 227064.

25 Z.-C. Jian, J.-X. Guo, Y.-F. Liu, Y.-F. Zhu, J. Wang and Y. Xiao, Cation Migration in Layered Oxide Cathodes for Sodium-Ion Batteries : Fundamental Failure Mechanisms and Practical Modulation Strategies, *Chem. Sci.*, 2024, **15**, 19698–19728, DOI: **10.1039/d4sc05206d**.

26 C. Jiang, Y. Wang, Y. Xin, X. Ding, S. Liu, Y. Pang, B. Chen, Y. Wang, L. L. Gao, F. Wu and H. Gao, Toward High Stability of O3−type NaNi$_{1/3}$Fe$_{1/3}$Mn$_{1/3}$O$_2$ Cathode Material with Zirconium Substitution for Advanced Sodium-Ion Batteries, *Carbon Neutralization*, 2024, **3**, 233–244, DOI: **10.1002/cnl2.115**.